Exploring quantum phases by driven dissipation

Nicolai Lang* and Hans Peter Büchler
Institute for Theoretical Physics III, University of Stuttgart, 70550 Stuttgart, Germany
(Received 25 November 2014; published 29 July 2015)

Dephasing and decay are the intrinsic dissipative processes prevalent in any open quantum system and the dominant mechanisms for the loss of coherence and entanglement. This inadvertent effect not only can be overcome but can even be capitalized on in a dissipative quantum simulation by means of tailored couplings between the quantum system and the environment. In this context it has been demonstrated that universal quantum computation can be performed using purely dissipative elements, and furthermore, the efficient preparation of highly entangled states is possible. In this article, we are interested in nonequilibrium phase transitions appearing in purely dissipative systems and the exploration of quantum phases in terms of a dissipative quantum simulation. To elucidate these concepts, we scrutinize exemplarily two paradigmatic models: the transverse-field Ising model and the considerably more complex $\mathbb{Z}_2$ lattice gauge theory. We show that the nonequilibrium phase diagrams parallel the quantum phase diagrams of the Hamiltonian "blueprint" theories.

DOI: 10.1103/PhysRevA.92.012128 PACS number(s): 03.65.Yz, 64.60.Ht, 05.30.Rt, 64.70.Tg

I. INTRODUCTION

Both dissipative quantum computation [1,2] and state preparation [3–5] are based on the description of the quantum system in terms of a Lindblad master equation. Both require the existence of a pure state as unique nonequilibrium steady state (NESS), which is a dark state of the dissipative coupling between system and bath; i.e., the state does not interact with the open reservoir. Especially the existence and uniqueness of the desired pure steady state are in general highly nontrivial tasks and often require a careful and sophisticated design of the coupling between system and bath. For example, it has been proven that any graph state can be prepared efficiently by dissipation [1,3], the latter being a resource for dissipative quantum computation. The first experimental proofs of principle of these ideas have been furnished quite recently with trapped ions [6,7]. In such experimental setups the implementation of theoretically well-designed couplings will be error-prone and, in general, lead to a mixed steady state. It is then a crucial question whether this nonequilibrium steady state is "close enough" to the desired pure dark state and still features the desired properties. First steps in this direction have been taken by analyzing the appearance of nonequilibrium phase transitions due to competing coherent and dissipative dynamics [8–21].

In this article, we study this question in a paradigmatic setup, where competing dissipative terms drive the system towards well-known pure quantum phases and, as a consequence, give rise to a nonequilibrium phase transition connecting them. The central idea is to start with *two* types of dissipative terms: the first one drives the system into a unique and pure nonequilibrium steady state, whereas the second type of dissipative coupling prefers steady states exhibiting true long-range order. We then analyze the nonequilibrium phase diagram depending on the relative coupling strength of the two dissipative baths. This analysis follows a mean-field treatment of the dissipative dynamics—which is valid in high dimensions. We derive the properties of the phase transition, as well as its critical exponents, and compare its behavior with the well-established thermal phase transition of the analog Hamiltonian theory. We argue that such purely dissipative quantum simulations can pave the way for the robust exploration of phase diagrams of complex quantum systems that are notoriously hard to tackle analytically. Building on these observations, we expand our concept and present a dissipative quantum simulation of the $\mathbb{Z}_2$ lattice gauge theory with a coupled matter field.

II. OPEN QUANTUM SYSTEMS

We start with a description of the time evolution of a generic quantum system coupled to a Markovian bath. Throughout this article we are interested in a purely dissipative dynamics governed by the Lindblad master equation [22],

$$\dot{\rho} = \sum_i \left[L_i \rho L_i^\dagger - \frac{1}{2}\{L_i^\dagger L_i, \rho\} \right] \equiv \mathcal{L}\rho, \tag{1}$$

with non-Hermitian jump operators $\{L_i\}$ characterizing the microscopic actions of the bath(s). Here ρ denotes the system density matrix, and $\{\cdot,\cdot\}$ the anticommutator. $\mathcal{L}$ is termed the *Lindblad superoperator* and generates the semigroup of completely positive trace-preserving maps $\exp(\mathcal{L}t)$ $(t \geqslant 0)$ which describes the time evolution via $\rho(t) = \exp(\mathcal{L}t)\rho_0$. Fixed points $\mathcal{L}\rho_{\mathrm{NESS}} = 0$ in the convex set of density matrices are usually referred to as *nonequilibrium steady states*; the pure ones $\rho_{\mathrm{NESS}} = |\Psi\rangle\langle\Psi|$, for which $L_i|\Psi\rangle = 0$ holds for all jump operators L_i, are particularly interesting and are called *dark states* [3]. The dynamics described by the Lindblad equation, (1), is completely determined by the jump operators $\{L_i\}$, the physical origin of which can be interpreted in various ways: From a microscopic angle they can be taken as the effective action of a Hamiltonian environment by tracing out its unitary dynamics and using the Born-Markov approximation (alongside additional assumptions) [23]. A different and more flexible point of view emerges in the field of digital quantum simulation [4,24,25], where the local jumps L_i are realized explicitly by the simulator in terms of local, tailored interactions. As we are interested in a *generic simulation* of

*nicolai@itp3.uni-stuttgart.de

quantum phases, we take the latter point of view and omit any microscopic realizations of the contrived jump operators. To this end we point out that a scheme for the microscopic simulation of arbitrary (local) jump operators was introduced in Ref. [4].

III. A PARADIGMATIC MODEL

We continue with a well-known model featuring a quantum phase transition: the transverse-field Ising model (TIM) [26]. The Hamiltonian for this paradigmatic theory on a D-dimensional (hyper-)cubic lattice with the spins located at sites $s \in \mathbb{S}$ reads

$$H_{\mathrm{TIM}} = -J \sum_{\langle s,t \rangle} \sigma_s^z \sigma_t^z - h \sum_s \sigma_s^x, \tag{2}$$

where $J \geqslant 0$ determines the nearest-neighbor coupling strength and h the transverse magnetic field. Here, σ_s^μ ($\mu = x,y,z$) are the Pauli matrices that act on spin s.

The appearance of a quantum phase transition and the properties of the different phases are well understood in the two limiting cases: for $h/J \to \infty$ we recover the disordered ground state $|+\rangle^{\mathbb{S}}$, which characterizes the *paramagnetic phase*, whereas for $h/J \to 0$ the system reaches the *ferromagnetic phase* with the twofold degenerate, symmetry-broken ground states $|\uparrow\rangle^{\mathbb{S}}$ and $|\downarrow\rangle^{\mathbb{S}}$.

These observations serve as a "blueprint" to construct a dissipative analog of the TIM. The main idea is to contrive two competing baths such that the dark states of the individual baths coincide with the ground states of the Hamiltonian theory in the above limiting cases. This concept allows us, first, to explore the quantum phases of the original Hamiltonian theory in a purely dissipative setup, and, second, to observe a nonequilibrium counterpart of the symmetry-breaking quantum phase transition mentioned above. The jump operators for the *dissipative TIM* take the form (an interpretation of their actions follows)

$$P_s = \sqrt{\kappa}\, \sigma_s^z \left[\mathbb{1} - \sigma_s^x\right] \quad \text{and} \tag{3a}$$

$$F_s = \sigma_s^x \left[\mathbb{1} - \frac{1}{q} \sum_{t \in s} \sigma_t^z \sigma_s^z\right] \equiv \sigma_s^x \left[\mathbb{1} - \sigma_{t\in s}^z \sigma_s^z\right], \tag{3b}$$

where $\kappa \geqslant 0$ is the relative coupling strength of the two baths (in analogy to the ratio h/J in the Hamiltonian theory). Here we have introduced the convenient notation $O_{t\in s} \equiv \frac{1}{|s|} \sum_{t\in s} O_t$, where $\sum_{t\in s}$ denotes the sum over all sites t adjacent to site s and $|s| = q = 2D$ denotes the number of nearest neighbors. Please note that the complete dissipative process $\{L_i\} = \{P_s, F_s\}$ decomposes into two competing baths of relative strength κ, the paramagnetic bath $\{P_s\}$ and the ferromagnetic bath $\{F_s\}$, each of which acts translationally invariant at all sites s. Clearly, the dissipative process $\{P_s, F_s\}$ inherits the global $\mathbb{Z}_2$ symmetry $U = \prod_s \sigma_s^x$ of the TIM, namely, $U L_s U^\dagger = e^{i\alpha} L_s, \alpha \in [0,2\pi)$ for all $L_s = P_s, F_s$. This setup is illustrated schematically in Fig. 1.

The construction of the jump operators in Eq. (3) follows the generic template

$$L = \text{Then} \cdot \text{If},$$

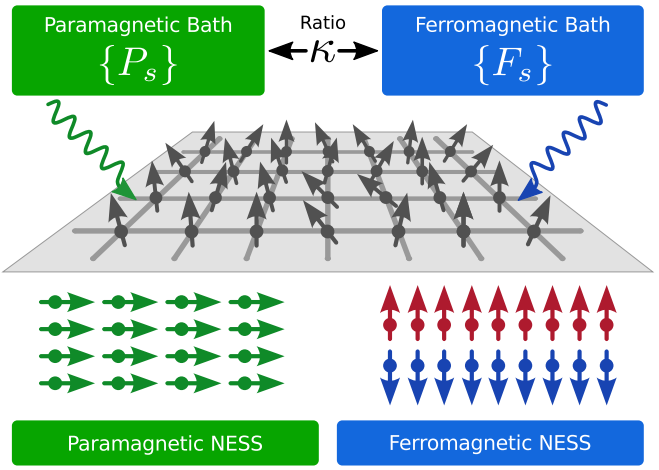

FIG. 1. (Color online) We consider a D-dimensional rectangular lattice with spins attached to the sites. The system is homogeneously coupled to *two* tailored Markovian baths with relative coupling strength κ. The $\{P_s\}$ ($\{F_s\}$) jump operators drive the system towards the paramagnetic (ferromagnetic) ground states of the transverse-field Ising model. There is *no* unitary dynamics involved.

where the If part "checks" whether some condition is met and the Then part applies a conditioned action thereupon. For the paramagnetic jump operators P_s this reads If $= \mathbb{1} - \sigma_s^x$, which probes whether the spin points along the magnetic field axis, and flips the spin otherwise via Then $= \sigma_s^z$, hence driving the system towards the disordered ground state $|+\rangle^{\mathbb{S}}$. The ferromagnetic jump operators F_s count the number of antiparallel neighbors via If $= \mathbb{1} - 1/q \sum_{t\in s} \sigma_t^z \sigma_s^z$ and condition thereby the spin flip Then $= \sigma_s^x$, driving towards the completely correlated ground states $\alpha|\uparrow\rangle^{\mathbb{S}} + \beta e^{i\phi}|\downarrow\rangle^{\mathbb{S}}$, where $|\alpha|^2 + |\beta|^2 = 1$ and $\phi \in [0,2\pi)$.

Along the lines of the Hamiltonian theory [where quantum phases are characterized by the ground state(s)], we are interested in the nonequilibrium steady states ρ_{NESS} of the dissipative theory with $\mathcal{L}\rho_{\mathrm{NESS}} = 0$, which characterize the nonequilibrium phases. It immediately follows from the design of the jump operators that in the limit $\kappa \to \infty$ the steady state is a unique dark state and coincides with the disordered pure state $\rho_{\mathrm{NESS}} = |+\rangle\langle+|^{\mathbb{S}}$, whereas for $\kappa \to 0$ the steady states are determined by the two symmetry-broken dark states $|\uparrow\rangle^{\mathbb{S}}$ and $|\downarrow\rangle^{\mathbb{S}}$, as well as coherent and incoherent mixtures thereof. In the latter case, all steady states exhibit long-range order $\langle \sigma_i^z \sigma_j^z \rangle = 1$ for $|i-j| \to \infty$—just as in the case of the Hamiltonian TIM. Finally, for a finite bath ratio ($0 < \kappa < \infty$) there are no dark states [27], and the system is driven towards a (unique, as simulations suggest) mixed steady state. It is therefore natural to ask whether there is a nontrivial dissipatively driven phase transition (in the thermodynamic limit) from a high-κ disordered to a low-κ ordered phase, which may be considered a nonequilibrium analog of the TIM phase transition.

IV. MEAN-FIELD THEORY

To tackle this question, we analyze the phase diagram of the driven dissipative TIM within mean-field theory, which will

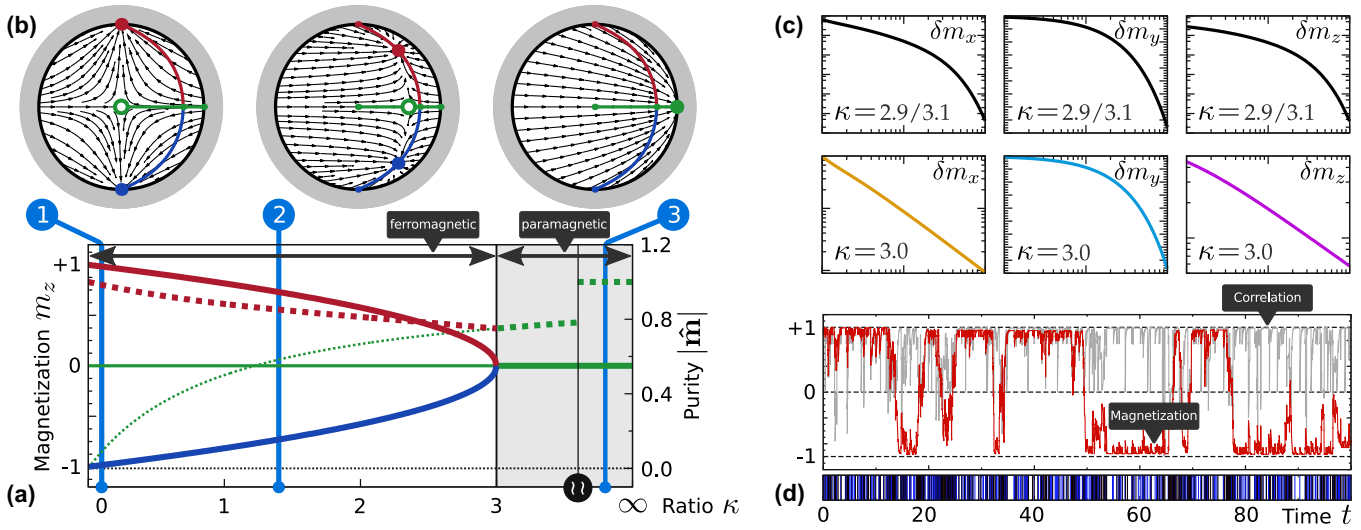

FIG. 2. (Color online) Results for the dissipative transverse-field Ising model. (a) Mean-field phase diagram. We show the magnetization m_z (solid lines) for all steady states as a function of κ (thick red and blue lines, stable ferromagnetic; thin green line, unstable paramagnetic; thick green line, stable paramagnetic]. The corresponding purities $|\hat{\mathbf{m}}|$ are illustrated by dashed lines of the same color and thickness. (b) Dynamical mean-field Lindblad flow $\mathbf{F}(\mathbf{m})$ in the m_x-m_z plane of the Bloch ball. Stable (unstable) steady states are labeled by bullets (circles); their paths for $0 \leqslant \kappa \leqslant \infty$ are highlighted. We illustrate the flow for three (1, 2, and 3) different ratios κ above and below the critical ratio $\kappa_c = 3$. (c) Relaxation of the Bloch vector $\mathbf{m}(t) = \delta\mathbf{m}(t) + \hat{\mathbf{m}}$ close to the steady state below, at, and above the critical ratio. The relaxation in the m_x and m_z direction becomes algebraic at the phase transition. (d) Quantum jump trajectory of a 3×3 instance with periodic boundary conditions in the ferromagnetic regime with $\sqrt{\kappa} = 1/3$. We show the average magnetization $1/9\langle\sum_s \sigma_s^z\rangle$ [red (dark) line] and the correlation $\langle\sigma_1^z\sigma_2^z\rangle$ [gray (light) line] starting from a completely polarized state $|\uparrow\rangle^{\otimes 9}$. Ferromagnetic (paramagnetic) jumps F_s (P_s) are encoded by blue (black) impulses in the lower part.

provide reliable results for large lattice dimensions D. The basic procedure to derive an effective mean-field description for Lindbladian theories is quite similar to the Hamiltonian counterpart [12]: We start with the product ansatz $\rho = \bigotimes_s \rho_s$ for the density matrix (ρ_s denotes a single-site density matrix) and insert it into the Lindblad equation, (1), thereby neglecting all spin-spin correlations. Tracing out the whole system except one spin (and assuming a homogeneous system) yields an effective Lindblad equation for a single spin,

$$\dot{\hat{\rho}} = \sum_{j=0}^{3}\left[f_j \hat{\rho} f_j^\dagger - \frac{1}{2}\{f_j^\dagger f_j, \hat{\rho}\}\right], \tag{4}$$

where we set $\hat{\rho} \equiv \rho_s$ to emphasize the homogeneity of the system (i.e., the dynamics of the whole system decouples into the same single-spin dynamics for each spin). The ferromagnetic jump operators give rise to three effective mean-field jump operators, namely,

$$f_1 = \sigma^x[\mathbb{1} - m_z\sigma^z],$$
$$f_2 = 1/\sqrt{2D}\,\sqrt{1 - m_z^2}\,\sigma^y, \quad \text{and}$$
$$f_3 = 1/\sqrt{2D}\,\sigma^z,$$

whereas the paramagnetic jump operator is not affected by the approximation, that is, $f_0 = \sqrt{\kappa}\,\sigma^z[\mathbb{1} - \sigma^x]$. Note that interacting jump operators (such as F_s) result in more than one mean-field jump operator (here $f_{1,2,3}$) which account for dephasing due to the adjacent jump operators of the same type. The expectation values $m_k \equiv \langle\sigma^k\rangle = \mathrm{Tr}\,[\hat{\rho}\sigma^k]$ ($k = x, y, z$) have to be determined self-consistently and thus render the mean-field master equation nonlinear in the single-spin density matrix $\hat{\rho} = (\mathbb{1} + \mathbf{m}\boldsymbol{\sigma})/2$ with the Bloch vector $\mathbf{m} = (m_x, m_y, m_z)$ restricted to $|\mathbf{m}| \leqslant 1$. Here self-consistency is ensured by identification of the expectation values $\langle\sigma^k\rangle$ and the Bloch vector components m_k.

It is convenient to rewrite the Lindblad equation, (4), in terms of a dynamical system

$$\partial_t \mathbf{m} = \mathbf{F}(\mathbf{m}) \tag{5}$$

with the nonlinear flow $\mathbf{F} : \mathbb{R}^3 \to \mathbb{R}^3$. The steady-state Bloch vectors $\hat{\mathbf{m}}$ are then determined by $\mathbf{F}(\hat{\mathbf{m}}) = 0$ and their stability (i.e., physical relevance) can be inferred from the negativity of the spectrum of the Jacobian matrix $\mathrm{D}\mathbf{F}(\hat{\mathbf{m}})$. For technical details we refer the reader to Appendix A.

V. RESULTS

The main results of the mean-field theory are outlined in Figs. 2(a)–2(c). We find a second-order phase transition for our purely dissipative replica of the TIM [see Fig. 2(a)]. For the critical mean-field ratio one obtains $\kappa_c = 4(1 - 1/q)$, which depends on the coordination number $q = 2D$ (see Appendix A). For $\kappa \geqslant \kappa_c$ there is a single (stable) fixed point of $\mathbf{F}$ as can be seen from the m_x-m_z cross section of the Bloch ball [Fig. 2(b)]. Starting from the correct paramagnetic dark state $|+\rangle$ for $\kappa = \infty$ [see (b3)], the steady state becomes mixed for $0 < \kappa < \infty$ but remains paramagnetic until at $\kappa = \kappa_c$ two additional ferromagnetic fixed points emerge. In the ferromagnetic regime $0 \leqslant \kappa < \kappa_c$ [see (b2)], the paramagnetic solution becomes unstable. The ferromagnetic solutions reach the correct dark states $|\uparrow\rangle$ and $|\downarrow\rangle$ for $\kappa \to 0$ [see (b1)]. At the

critical point we find the typical mean-field exponent $\beta = 1/2$, i.e., $|\hat{m}_z| = (1-\kappa/\kappa_c)^\beta$.

In addition, the Lindblad master equation, (5), provides information on the dynamics of the system and the time scales required to reach the steady state. Here we find a nonequilibrium critical slowing-down close to the phase transition [Fig. 2(c)]: Whereas above and below κ_c the system is damped exponentially close to the steady state, this decay turns out to be algebraic in the m_x and m_z directions at the phase transition, that is, $\delta m_k(t) \propto t^{\eta_k}$ $(k = x,z)$ for $|\delta m_k| \ll 1$ (or $t \to \infty$) with the exponents $\eta_x = -1$ and $\eta_z = -1/2$. We point out that the algebraic relaxation in the m_z direction with $\eta_z = -1/2$ is an immediate consequence of a vanishing eigenvalue of the Jacobian matrix $D\mathbf{F}$ (for $\kappa \neq \kappa_c$ it is negative-definite). In contrast, the algebraic relaxation in the m_x direction with $\eta_x = -1$ results from the coupling of m_z and m_x in Eq. (5) and different relaxation rates in the m_x and m_z directions.

These results parallel the well-known mean-field theory for the TIM at finite temperatures [since the steady state is mixed at the phase transition; see Fig. 2(a)]. Nevertheless, this is a nonequilibrium phase transition connecting the two zero-temperature quantum phases of the TIM via a nonthermal manifold of states.

VI. MONTE CARLO SIMULATION

In order to demonstrate the competitive nature of the baths $\{P_s\}$ and $\{F_s\}$—which is a key ingredient for the nonequilibrium phase transition—we performed quantum trajectory Monte Carlo simulations in small setups [23,28,29]. A typical quantum jump trajectory for a 3×3 lattice with periodic boundary conditions is shown in Fig. 2(d). The initial state was completely m_z polarized, $|\Psi_0\rangle = |\uparrow\rangle^{\otimes 9}$, and the bath ratio $\sqrt{\kappa} = 1/3$ deep in the ferromagnetic regime. We show the average polarization $1/9\langle\sum_s \sigma_s^z\rangle$ [red (dark) line] and the nearest-neighbor correlation $\langle\sigma_1^z\sigma_2^z\rangle$ [gray (light) line]. The ferromagnetic (paramagnetic) jumps F_s (P_s) are encoded by blue (black) impulses at the bottom.

The finite correlations—combated by paramagnetic jumps—indicate the emergence of local order due to the ferromagnetic driving. As a finite-size artifact, we observe a dynamically bistable behavior of the polarization due to the competition of (dominant) ferromagnetic jumps stabilizing the plateaus and weak paramagnetic jumps responsible for the global polarization inversions. The latter are paralleled by an increased jump rate as the jump history reveals (black clusters). Such intermittent fluctuations of the jump rate are a well-known phenomenon of dynamical phase transitions in dissipative setups [16,19,30]. In the paramagnetic regime, the correlations vanish with $\kappa \to \infty$ due to frequent paramagnetic jumps, and the initial m_z polarization is lost rapidly. These observations support our claim of a nonequilibrium phase transition motivated by mean-field calculations—although the small system sizes render any definite conclusion impossible.

Let us close this first part with a short résumé: We have introduced a dissipative version of the transverse-field Ising model and shown that (1) we can probe the pure quantum phases of the Hamiltonian theory in the limiting regimes and (2) the mean-field theory predicts a nonequilibrium counterpart of the order-disorder phase transition. Succeeding with this paradigmatic model raises the question whether more complex theories allow for an analogous dissipative mimicry to probe their quantum phases and find interesting nonequilibrium phase transitions. We answer in the affirmative, introducing the dissipative $\mathbb{Z}_2$-Gauge-Higgs ($\mathbb{Z}_2$GH) model.

VII. DISSIPATIVE $\mathbb{Z}_2$-GAUGE-HIGGS MODEL

Motivated by the possibility of exploring quantum phases with driven dissipation, we present a dissipative implementation of the famous $\mathbb{Z}_2$GH model [31–33]. Recently there has been intensified interest in the quantum simulation of gauge theories [34–36], where the focus so far lies on the robust realization of the gauge constraints. Here we focus *not* on the latter but on the dynamics within the gauge-invariant sector itself. To this end, consider a D-dimensional rectangular lattice with spin-1/2 representations attached to sites s (the *matter field*; denoted σ_s^k) and edges e (the *gauge field*; denoted τ_e^k). Here, σ_s^k and τ_e^k $(k = x,y,z)$ denote Pauli matrices. Then the Hamiltonian of the $\mathbb{Z}_2$GH model reads

$$H_{\mathbb{Z}_2\mathrm{GH}} = -\sum_s \sigma_s^x - \lambda \sum_e I_e - \sum_e \tau_e^x - \omega \sum_p B_p, \quad (6)$$

where subscripts s, e, and p denote sites, edges and faces of the (hyper-)cubic lattice, respectively; ω and λ are non-negative real parameters. The plaquette operators $B_p \equiv \prod_{e\in p} \tau_e^z$ describe a four-body interaction of gauge spins on the perimeter of face p and $I_e \equiv \sigma_{s_1}^z \tau_e^z \sigma_{s_2}^z$ (where $e = \{s_1,s_2\}$) realizes a gauged Ising interaction between adjacent matter spins. Note that $H_{\mathbb{Z}_2\mathrm{GH}}$ features the *local* gauge symmetry $G_s \equiv \sigma_s^x \prod_{e;s\in e} \tau_e^x = \sigma_s^x A_s$, i.e., $[H,G_s] = 0$ for all sites s. Here $A_s \equiv \prod_{e:s\in e} \tau_e^x$ denotes a $2D$-body interaction of gauge spins located on the edges adjacent to site s.

The expected quantum phase diagram in $2+1$ dimensions is sketched in Fig. 3(a) and features three distinct phases [33,37]: the (I) confined charge, (II) free charge, and (III) Higgs phases. To contrive a family of baths that explore these three phases and give rise to a nonequilibrium analogy of Fig. 3(a), it proves advantageous to analyze the elementary excitations of $H_{\mathbb{Z}_2\mathrm{GH}}$ in the three parameter regimes: We aim at jump operators that remove the elementary excitations of each phase and thereby drive the system towards the latter. In addition, this scheme leads inevitably to gauge-invariant jump operators L, i.e., $[L,G_s] = 0$ for all sites s—which is a necessary condition for the intended gauge-symmetry constrained dynamics. We stress that any realistic implementation would have to deal with gauge-symmetry-violating imperfections, demanding additional mechanisms to enforce gauge invariance [34,35].

For the sake of brevity, we label localized excitations ("quasiparticles") by the corresponding operator in Hamiltonian (6) and its eigenvalue. For example, $\sigma_s^x = -1$ refers to a state $|\chi\rangle$ such that $\sigma_s^x|\chi\rangle = -|\chi\rangle$ and we say that $|\chi\rangle$ describes a system with an (electric) charge at site s.

We start with the confined charge phase (I) for $\lambda,\omega \to 0$. The Hamiltonian reads $H_{\mathbb{Z}_2\mathrm{GH}} = -\sum_s \sigma_s^x - \sum_e \tau_e^x$ and the elementary excitations are charges $\sigma_s^x = -1$ and gauge strings $\tau_s^x = -1$. The physically admissible, that is, gauge-invariant

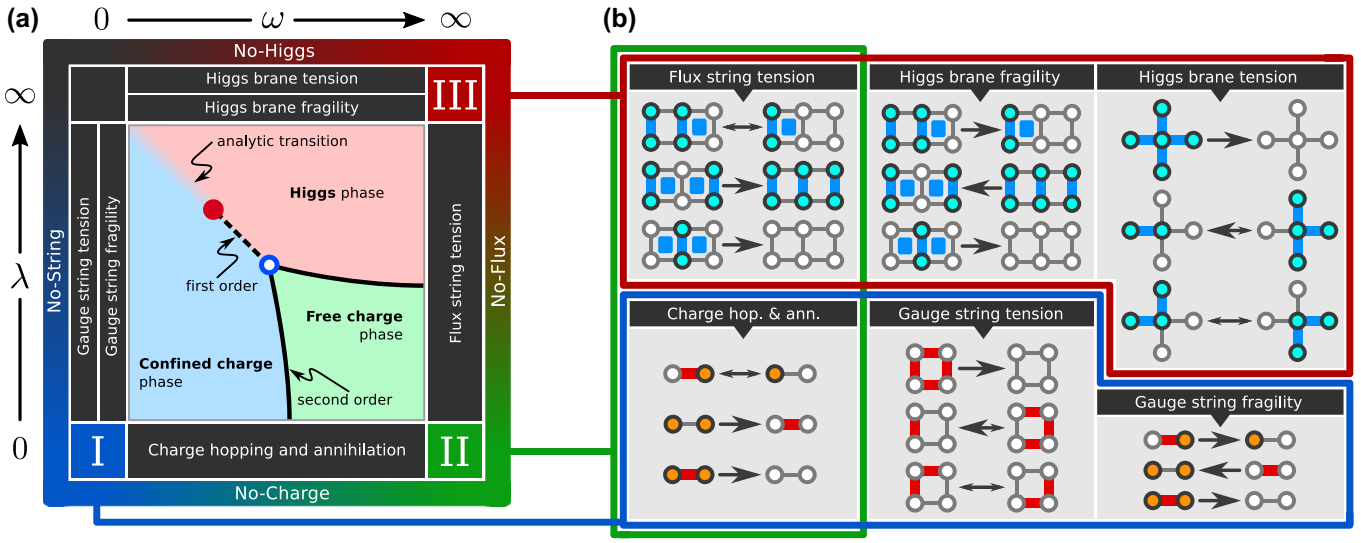

FIG. 3. (Color online) Conceptual foundation of the dissipative $\mathbb{Z}_2$-Gauge-Higgs model. (a) Qualitative illustration of the well-known phase diagram of the Hamiltonian $\mathbb{Z}_2$-Gauge-Higgs theory in the ω-λ plane. There are three characteristic phases: the (I) confined charge, (II) free charge, and (III) Higgs phases. In order to drive the system dissipatively in a distinct phase, combinations of the baths adjacent to the labels I, II, and III are employed. (b) Effects of the six types of jump operators (characterizing the baths) on elementary excitations in two spatial dimensions. Asymmetric arrows denote asymmetric quantum jump probabilities. The symbols in the lower three boxes read as follows: yellow (dark) site $\Leftrightarrow \sigma^x = -1$ (electric charge); red (thick) edge $\Leftrightarrow \tau^x = -1$ (gauge string). In the upper three boxes: blue (dark) site + (thick) edge $\Leftrightarrow I_e = -1$ (Higgs excitation); blue (filled) face $\Leftrightarrow B_p = -1$ (magnetic flux). The formal definitions are listed in Table I.

excitations are generated by I_e and B_p, where I_e creates a pair of charges on adjacent sites connected by a gauge string (usually called a *meson*) and B_p gives rise to a closed gauge string on the perimeter of p. We conclude that physical states are characterized by (1) closed gauge strings and (2) open gauge strings with charges attached to their end points. Such states obey a Gauss-like law, $G_s|\chi\rangle = |\chi\rangle$ for all s, which restricts the physical states to the gauge-invariant subspace of the complete Hilbert space characterized by $\sigma_s^x A_s = \mathbb{1}$. Note that the energy for separating two charges grows linearly with their distance since gauge strings are penalized by the Hamiltonian; thus the charges are confined, which gives rise to the name *confined charge phase*.

Let us now shift attention to the dissipative analog theory. To get rid of an arbitrary configuration of charges (confined by gauge strings) and gauge loops, a gauge-symmetric dissipative process must (1) contract gauge strings, (2) annihilate pairs of charges, and (3) break gauge loops by creating mesons. The latter is only necessary for systems with nontrivial spatial topology, e.g., systems with periodic boundary conditions. We end up with the three baths *charge hopping and annihilation*, *gauge string tension*, and *gauge string fragility* [see Fig. 3(b) for a pictorial description and Table I for formal definitions of the jump operators].

We proceed with the discussion of the remaining two phases. The free charge phase (II) is characterized by $\lambda \to 0$ and $\omega \to \infty$ and the system is described by $H_{\mathbb{Z}_2\mathrm{GH}} = -\sum_s \sigma_s^x - \omega \sum_p B_p$. Clearly, the matter and the gauge field decouple and the elementary excitations are charges $\sigma_s^x = -1$ and magnetic fluxes $B_p = -1$ as excitations of the gauge string condensate. The latter appear as deconfined magnetic monopoles in $D = 2$ at the end of dual τ_e^x strings and as closed magnetic flux strings in $D = 3$ on the perimeter of dual τ_e^x planes [38]. Note that the charges are still created in pairs by I_e chains; the connecting gauge strings, however, are no longer penalized, hence the *free* charge phase. We conclude that the jump operators must provide mechanisms (1) to diffuse and annihilate charges and (2) to do the same with magnetic monopoles in $D = 2$ and contract magnetic flux strings in $D = 3$. This leads us to the already known charge hopping and annihilation and the new *flux string tension* (which degenerates in $D = 2$ to "monopole hopping and annihilation") [see Fig. 3(b) and Table I].

Finally, the Higgs phase (III) is reached for $\lambda, \omega \to \infty$ and the Hamiltonian reads $H_{\mathbb{Z}_2\mathrm{GH}} = -\lambda \sum_e I_e - \omega \sum_p B_p$. The elementary excitations are Higgs excitations $I_e = -1$ and flux strings $B_p = -1$. Pure Higgs excitations can be created by

TABLE I. Jump operators for the dissipative $\mathbb{Z}_2$-Gauge-Higgs model. Their action is described in the text. Pictorial descriptions are shown in Fig. 3. Subscripts s, e, and p denote sites, edges, and faces, respectively. The shorthand notation $e \in p$ denotes the normalized sum over all edges e adjacent to face p. The free parameters of the theory are labeled η_i for $i = 1, \ldots, 6$. The second column lists the jump operators of the gauge theory with nontrivial gauge condition $\sigma_s^x A_s = \mathbb{1}$.

Bath	Jump operator
Gauge string tension	$F_p^{(1)} = \eta_1 B_p(\mathbb{1} - \tau_{e\in p}^x)$
Gauge string fragility	$F_e^{(2)} = \eta_2 I_e(\mathbb{1} - \tau_e^x)$
Higgs brane tension	$D_s^{(1)} = \eta_3 \sigma_s^x(\mathbb{1} - I_{e\in s})$
Higgs brane fragility	$D_e^{(2)} = \eta_4 \tau_e^x(\mathbb{1} - I_e)$
Charge hopping & annihilation	$T_e = \eta_5 I_e(\mathbb{1} - \sigma_{s\in e}^x)$
Flux string tension	$B_e = \eta_6 \tau_e^x(\mathbb{1} - B_{p\in e})$

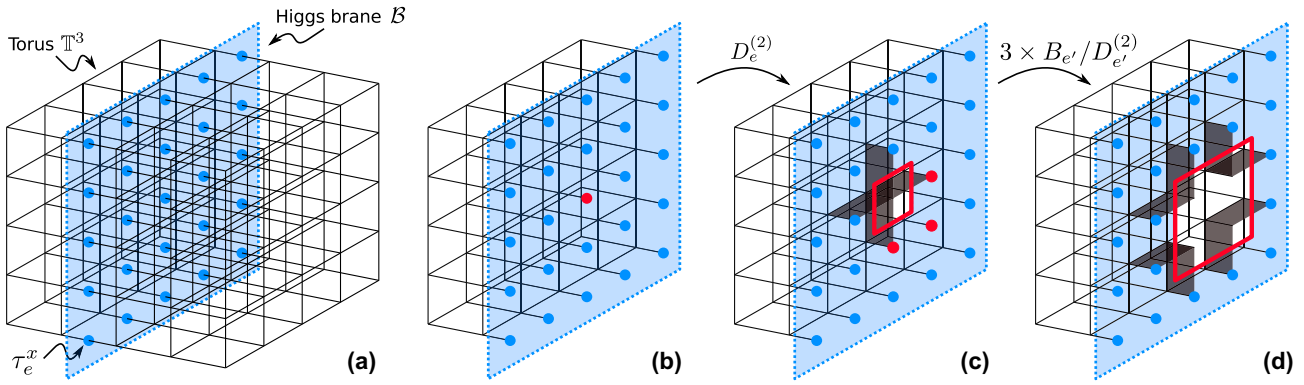

FIG. 4. (Color online) Action of the Higgs brane fragility $D_e^{(2)}$ and the flux string tension B_e in three spatial dimensions. (a) Closed dual plane (Higgs brane) $\mathcal{B}$ on the three-dimensional torus $\mathbb{T}^3$, which defines the topologically nontrivial brane operator $\prod_{e\in\mathcal{B}} \tau_e^x$ (filled blue circles). Such excitations cannot be annihilated by the Higgs brane tension $D_s^{(1)}$ and flux string tension B_e since $\mathcal{B}$ wraps once around the torus and there are no flux strings present. (b)–(d) A cross section of the lattice parallel to $\mathcal{B}$; we show the first few jumps to get rid of the excitations. (b) A Higgs brane fragility jump $D_e^{(2)}$ acts on the red edge e. (c) The Higgs excitation $I_e = -1$ is no longer present. One has to pay for this with four magnetic fluxes $B_p = -1$ on the adjacent faces $p \in e$ (black plaquettes). The latter define a flux loop (red line). (d) Three applications of the flux string tension $B_{e'}$ and/or Higgs brane fragility $D_{e'}^{(2)}$ on the edges e' (filled red circles) enlarge the hole in the Higgs brane. This process allows the retraction and subsequent annihilation of the formerly closed Higgs brane around the torus.

σ_s^x and form dual loops in $D = 2$ and closed dual surfaces ("branes") in $D = 3$. Flux strings can be created by dual strings of τ_e^x or dual planes with boundary of τ_e^x in $D = 3$. That is, magnetic fluxes (as monopoles in $D = 2$ or flux strings in $D = 3$) mark the boundary of (dual) Higgs excitation manifolds, i.e., open strings in $D = 2$ and open branes in $D = 3$. Since in two dimensions the flux strings degenerate to magnetic monopoles, the physics becomes dual to the free charge phase (I) via the identifications $\sigma_s^x \leftrightarrow B_p$ and $\tau_e^x \leftrightarrow I_e$. This duality should be preserved in our analogous dissipative setup. Appropriate dissipative processes must (1) get rid of the flux strings or monopoles and (2) eliminate the Higgs excitations. We handle the flux strings or monopoles by the already known flux string tension and introduce two new baths, the *Higgs brane tension* and the *Higgs brane fragility*, to eliminate pure Higgs excitations. Since Higgs excitations can be created by both σ_s^x and τ_e^x, in the form of closed branes, the latter must be contracted and cut in order to vanish on nontrivial topologies. The cutting of Higgs branes is indeed necessary in three dimensions since topologically nontrivial, dual brane operators $\prod_{e\in\mathcal{B}} \tau_e^x$ ($\mathcal{B}$ is a dual plane that winds once around the torus $\mathbb{T}^3$) create excitation patterns that can only be annihilated by "piercing holes" in the Higgs brane to retract it about $\mathbb{T}^3$ (see Fig. 4). The above-mentioned duality in two dimensions becomes manifest in the duality relating Higgs brane fragility and gauge string fragility. This becomes particularly clear in the ($D = 2$) pictorial representations in Fig. 3(b).

At this point it seems advisable to stress the differences between the Hamiltonian theory and its dissipative counterpart. Ground states of the Hamiltonian theory minimize the free energy or, at zero temperature, the energy of the system. To reach, say, the quantum phase at $T = 0$, the Hamiltonian system is coupled to a thermal bath whose temperature is gradually reduced towards 0. The cooling of the system is driven by thermal fluctuations which are conditioned according their Boltzmann weight with respect to the system Hamiltonian. It is important to stress that whether a certain transformation occurs (e.g., the breaking of a gauge loop into an open gauge string with charges terminating the strings) depends solely on its energetic effect with respect to the Hamiltonian. In contrast, there is no such thing as energy in the dissipative nonequilibrium setup. Consequently, the options for microscopic fluctuations are much more constrained, namely, by the possible actions of the jump operators. *Dissipative fluctuations are transformation selective, whereas thermal fluctuations are energy selective.* Consider once again the breaking of gauge loops: In a (thermal) Hamiltonian theory they will just break whenever it is energetically favorable. In our purely dissipative setup they can only break if we allow them to do so, that is, if we provide an appropriately designed bath with jump operators that break strings (in our case this bath is termed gauge string fragility and controlled by the parameter η_2; see Table I). In a nutshell, the translation of Hamiltonian "blueprint" theories into a purely dissipative nonequilibrium framework allows for much more fine-tuning at the microscopic level.

The relative bath strengths η_i, $i = 1,\ldots,6$ (see Table I), are free parameters of our theory and allow for the mentioned fine-tuning of the microscopic mechanisms. For instance, there is no *a priori* statement about the importance of "gauge string breaking" compared to "gauge string tension", and the influence of such ratios on the phase diagram is highly nontrivial. However, in the following we set $\eta_{1,2} = 1 = \eta_5$, $\eta_{3,4} = \sqrt{\lambda}$, and $\eta_6 = \sqrt{\omega}$ since this seems a natural choice to mimic the original theory, (6).

VIII. MEAN-FIELD ANALYSIS OF THE DISSIPATIVE $\mathbb{Z}_2$-GAUGE-HIGGS MODEL

To put the theory into operation and catch a glimpse of its qualitative phase diagram, we once again utilize a mean-field approach. Mean-field approximations for theories with (unphysical) gauge degrees of freedom are well known to yield not only quantitatively poor but also qualitatively wrong results [39–41]. However, we can test the ability of our dissipative $\mathbb{Z}_2$GH model to realize the different quantum phases of the Hamiltonian $\mathbb{Z}_2$GH theory by comparing the

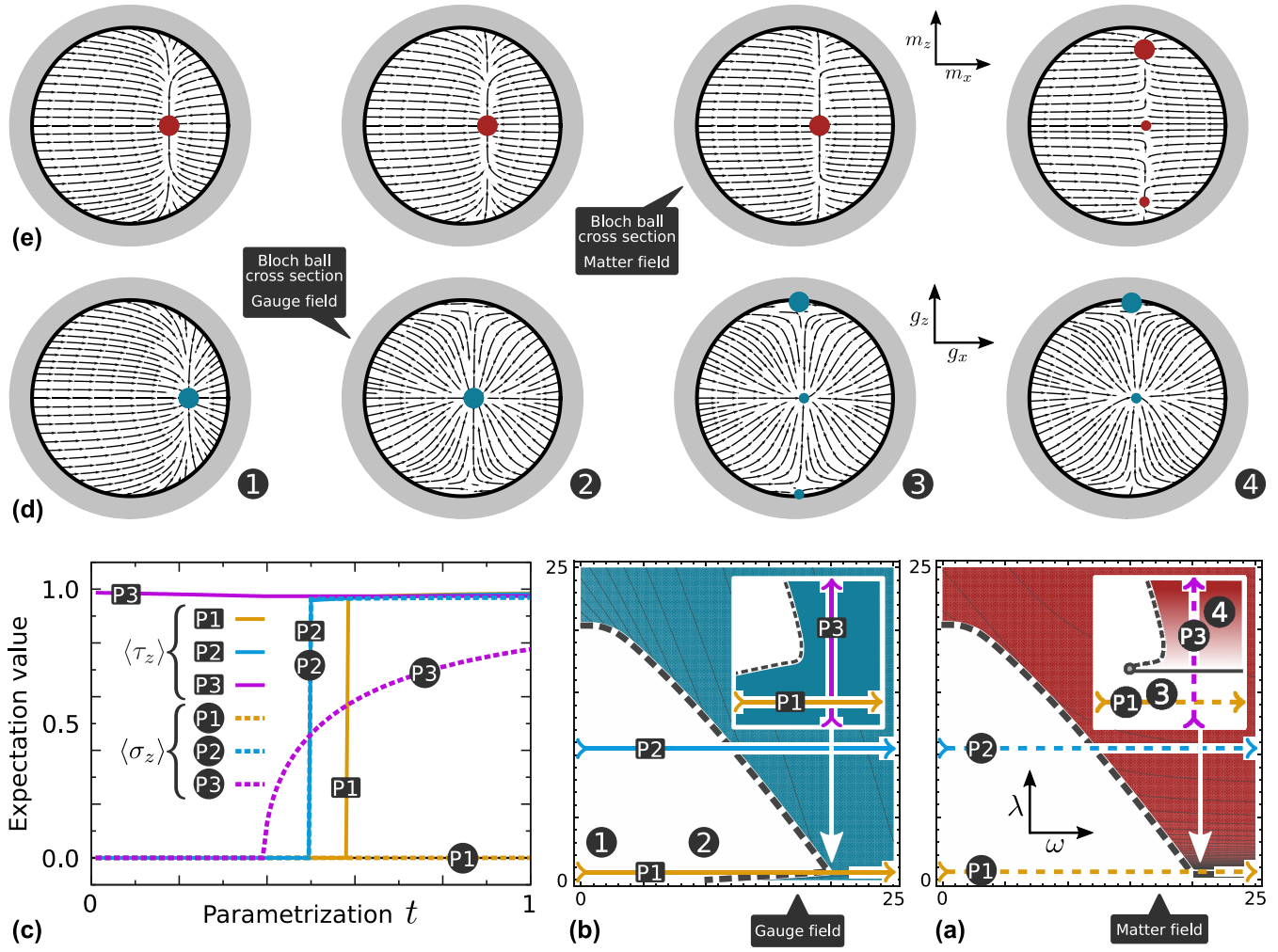

FIG. 5. (Color online) Mean-field phase diagram for the dissipative $\mathbb{Z}_2$-Gauge-Higgs model with two separate mean fields. (a) Plot of the maximal z polarization $\langle\sigma^z\rangle$ of all stable physical steady states for the matter field color-coded in the ω-λ plane (light $\rightarrow \langle\sigma^z\rangle = 0$, dark $\rightarrow \langle\sigma^z\rangle = 1$). (b) The same for the gauge field, that is, $\langle\tau^z\rangle$. (c) Quantitative results for $\langle\tau^z\rangle$ (solid lines) and $\langle\sigma^z\rangle$ (dashed lines) on the colored and labeled paths in (b) and (a). (d), (e) Cross sections of the Bloch ball (g_x/m_x-g_z/m_z plane) for the gauge field (d) and matter field (e) with the dynamical mean-field flow $\mathbf{F}$ as flux lines and the stable physical fixed points shown by (small and large) circles. The corresponding parameters (ω,λ) for each vertical pair of cross sections are highlighted by numbers in the 2D plots (a), (b). The flux lines shown for the Bloch vector of one mean field depend on the Bloch vector of the other since the mean-field equations couple all six degrees of freedom. Each depicted gauge-field flux corresponds to a fixed-point Bloch vector for the corresponding matter field, and vice versa (shown by large red and cyan circles). A discussion of the results is given in the text.

predictions of both models within mean-field theory, where the features and shortcomings of the Hamiltonian $\mathbb{Z}_2$GH model are well established [39,40].

We followed two mean-field approaches, the combination of which is known to capture all essential features of the quantum phase diagram for the Hamiltonian theory. The results for one of these approaches are shown in Fig. 5 and we find that they correspond qualitatively to the results of the Hamiltonian counterpart. An alternative approach in unitary gauge is discussed in Appendix B.

Here we present the simplest approach to obtain an effective mean-field description of the theory by introducing two independent mean field degrees of freedom. That is, we make the ansatz

$$\rho = \bigotimes_{e\in\mathbb{E}} \rho_e^{\mathrm{g}} \otimes \bigotimes_{s\in\mathbb{S}} \rho_s^{\mathrm{m}} \tag{7}$$

for the density matrix, where $\rho_e^{\mathrm{g}} = (\mathbb{1}_e + \mathbf{g}\boldsymbol{\tau}_e)/2$ describes the single-site gauge field with Bloch vector $\mathbf{g} = (g_x,g_y,g_z)$, and $\rho_s^{\mathrm{m}} = (\mathbb{1}_s + \mathbf{m}\boldsymbol{\sigma}_s)/2$ analogously the matter field with Bloch vector $\mathbf{m} = (m_x,m_y,m_z)$. Self-consistency once again demands $g_k = \langle\tau_e^k\rangle$ and $m_k = \langle\sigma_s^k\rangle$ for $k = x,y,z$; assuming a homogeneous system allows us to omit the site and edge indices. A treatment analogous to that in the case of the dissipative TIM yields a nonlinear dynamical system with the six-dimensional flow $\mathbf{F}(\mathbf{g},\mathbf{m}) = (\mathbf{F}^{\mathrm{g}},\mathbf{F}^{\mathrm{m}})$, namely,

$$\partial_t \mathbf{g} = \mathbf{F}^{\mathrm{g}}(\mathbf{g},\mathbf{m}) \quad \text{and} \quad \partial_t \mathbf{m} = \mathbf{F}^{\mathrm{m}}(\mathbf{g},\mathbf{m})\,. \tag{8}$$

Stationary states (NESS) can be determined by solving the nonlinear system of equations $\mathbf{F}^{\mathrm{g}}(\hat{\mathbf{g}},\hat{\mathbf{m}}) = 0 = \mathbf{F}^{\mathrm{m}}(\hat{\mathbf{g}},\hat{\mathbf{m}})$ and their stability can be inferred from the spectrum of $\mathrm{D}\mathbf{F}(\hat{\mathbf{g}},\hat{\mathbf{m}})$.

The results are shown in Fig. 5. In Figs. 5(a) and 5(b) we illustrate the expectation values $m_z = \langle\sigma^z\rangle$ and $g_z = \langle\tau^z\rangle$ for

the matter and the gauge fields, respectively; Fig. 5(c) shows these quantities on the three highlighted paths. In the case of multiple stable solutions, we choose the one which maximizes first g_z and then m_z. For the Hamiltonian mean-field approach such a selection can be justified by comparing the free energies of all possible solutions. Lacking an extremum principle in the nonequilibrium setting, it remains an open question which solutions are truly stable and which, in contrast, give rise to metastable states (or do not exist at all).

Nevertheless, we find three distinct phases, characterized by the existence of solutions with $m_z = 0 = g_z$ (1 and 2), $m_z = 0 \neq g_z$ (3), and $m_z \neq 0 \neq g_z$ (4). They can be identified as the confined charge, free charge, and Higgs phases, respectively. There are two types of phase transitions present [see Fig. 5(c)]. The confined charge phase is separated from the other two phases by a first-order transition, which is indicated by a jump $g_z = 0 \to g_z > 0$; the transition between the free charge and the Higgs phase is of second order and indicated by a continuous transition $m_z = 0 \nearrow m_z > 0$.

We have to lower our sights regarding the graphical representation of the six-dimensional mean-field flow $\mathbf{F}(\mathbf{g},\mathbf{m}) = (\mathbf{F}^{\mathrm{g}},\mathbf{F}^{\mathrm{m}})$ in Figs. 5(d) and 5(e). Here we show (the projection of) $\mathbf{F}^{\mathrm{g}}(\mathbf{g},\hat{\mathbf{m}})$ in Fig. 5(d) and $\mathbf{F}^{\mathrm{m}}(\hat{\mathbf{g}},\mathbf{m})$ in Fig. 5(e) for the fixed points $\hat{\mathbf{g}}$ and $\hat{\mathbf{m}}$ shown by large circles in the corresponding cross section. Other stable fixed points are shown by small circles of the same color. In the confined charge phase there is a unique stable fixed point; see (1) and (2). In the free charge phase two additional stable fixed points emerge close to the $g_z = \pm 1$ poles which are responsible for the first-order phase transition. All three stable solutions correspond to a vanishing matter field $m_z = 0$. In the Higgs phase the solution close to the $g_z = -1$ pole vanishes and only the ones close to $g_z = 0$ and $g_z = 1$ remain. There are three solutions, namely, $g_z = 0 = m_z$, $g_z > 0 < m_z$, and $g_z > 0 > m_z$. That the solutions of the gauge field are not symmetric about the g_x axis (horizontal axis in the cross sections), whereas the matter-field solutions feature this symmetry about the m_x axis, is related to the fact that the theory features the global symmetry $\prod_s \sigma_s^x = \prod_s G_s$ but not an analogous symmetry $\prod_e \tau_e^x$ for the gauge field.

An obvious drawback of this mean-field approach is that the gauge degrees of freedom are not fixed and are erroneously treated as physical degrees of freedom. This leads to the well-known artifact that the analytical path connecting confined charge and Higgs phase is lost. However, the theory predicts all three phases correctly.

To properly exclude unphysical (gauge) degrees of freedom, it proves advantageous to localize the latter on distinguished subsystems—which then decouple from the gauge-invariant dynamics and can be dropped in mean-field considerations. This can be achieved in unitary gauge where the physical subspace $\mathcal{H}_{\mathbb{Z}_2\mathrm{GH}} = \{|\Psi\rangle \,|\, G_s = \mathbb{1}\}$ is unitarily rotated into the new subspace $\tilde{\mathcal{H}}_{\mathbb{Z}_2\mathrm{GH}} = \{|\Psi\rangle \,|\, \sigma_s^x = \mathbb{1}\} = T\mathcal{H}_{\mathbb{Z}_2\mathrm{GH}}$ via T. Then one finds a first-order phase transition separating the confined charge and free charge and Higgs phases—the latter two no longer being distinct. In contrast to our approach above, the first-order line terminates at a critical point (ω_c,λ_c) and the analytical transition of Fig. 3(a) is recovered within mean-field theory. These results once again parallel the already known mean-field phase diagram of the Hamiltonian theory in unitary gauge [39,40]. For a detailed discussion the reader is referred to Appendix B.

IX. CONCLUSION

In this article we have introduced the mimicry of well-known (quantum) phase transitions by Markovian nonequilibrium systems. We have illustrated the construction of competing baths for a simple paradigmatic system—the transverse-field Ising model—and the considerably more complex $\mathbb{Z}_2$ lattice gauge theory with a coupled matter field. For this purpose we employed the Hamiltonian versions of the theories as "blueprints" to come up with appropriate jump operators that drive the dissipative system towards the pure quantum phases of the Hamiltonian theory. We have pointed out that the nonequilibrium framework can be seen as a "construction kit" for nonthermal phase transitions that features typically more parameters and thus more versatile control over the microscopic behavior than the original Hamiltonian theory. It is an interesting open question to what extent the potentially much richer nonthermal manifold of states can be probed in this fashion. We believe that such purely dissipative quantum simulations can serve as a new, generic, and inherently robust tool for the exploration of otherwise inaccessible phase diagrams of complex quantum systems.

ACKNOWLEDGMENTS

We thank J. K. Pachos for inspiring discussions. We acknowledge support from the Center for Integrated Quantum Science and Technology (IQST) and the Deutsche Forschungsgemeinschaft (DFG) within SFB TRR 21. N.L. thanks the German National Academic Foundation for their support.

APPENDIX A: MEAN-FIELD THEORY FOR LINDBLAD MASTER EQUATIONS

1. Mean-field jump operators

Let the system's states be described by the N-spin Hilbert space $\mathcal{H}_N = \bigotimes_{i=1}^N \mathbb{C}_i^2$. For mean-field theory we choose the ansatz $\rho = \bigotimes_l \rho_l$, where ρ_l is the density matrix of a single spin degree of freedom. Here we consider the generic case, that is, we allow for $1 \leqslant M \leqslant N$ independent spins in the mean-field description. For example, for $M = 1$ we end up with a completely homogeneous system; $M = N$ describes a system of N distinguished spins which are incoherently coupled to their neighbors via their expectation values. Usually one will choose $O(1)$ mean fields to assign a distinct mean-field degree of freedom to all distinguished fields in the exact theory [42].

Given M mean fields, the density matrix reads $\rho^{\mathrm{mf}} = \bigotimes_{\alpha=1}^M \tilde{\rho}_\alpha$, where $\tilde{\rho}_\alpha$ describes the (homogeneous) αth mean field. The effective jump operators are obtained by tracing out selectively all degrees of freedom but one, meaning

$$\partial_t \tilde{\rho}_\alpha = \partial_t \,\mathrm{Tr}_{\neq m}\,[\rho] = \mathrm{Tr}_{\neq m}\,[\mathcal{L}[\rho]], \tag{A1}$$

where $1 \leqslant m \leqslant N$ is a physical spin which represents the field of type α. The dynamics of the mean-field spins $\{\tilde{\rho}_\alpha\}$ is

described by effective Lindblad equations

$$\partial_t \tilde{\rho}_\alpha = \sum_i \sum_{\mu_i} \left[l^\alpha_{i,\mu_i} \tilde{\rho}_\alpha l^{\alpha\dagger}_{i,\mu_i} - \frac{1}{2}\left\{ l^{\alpha\dagger}_{i,\mu_i} l^\alpha_{i,\mu_i}, \tilde{\rho}_\alpha \right\} \right], \tag{A2}$$

where one has to keep in mind that these equations are nonlinear due to the mean fields included in the effective jump operators:

$$L_i \xrightarrow{\alpha} \left\{ l^\alpha_{i,\mu_i} \right\}_{\mu_i} = \left\{ l^\alpha_{i,\mu_i}\left(\left\{ m^k_\beta \right\} \right) \right\}_{\mu_i}. \tag{A3}$$

Here $m^k_\beta \equiv \langle \sigma^k_\beta \rangle = \mathrm{Tr}\left[\sigma^k_\beta \tilde{\rho}_\beta\right]$ denotes the kth component of the βth mean field ($k = x,y,z$). Furthermore, note that for each exact jump operator L_i there may be several effective jump operators l^α_{i,μ_i} with $\mu_i = 1,2,3,\ldots$ for each mean field α.

For the sake of simplicity we employ a resummation and redefinition of the effective jump operators to get rid of duplicates (which usually occur due to structural symmetries of the lattice). So rewrite Eq. (A2) as

$$\partial_t \tilde{\rho}_\alpha = \sum_\mu \left[l^\alpha_\mu \tilde{\rho}_\alpha l^{\alpha\dagger}_\mu - \frac{1}{2}\left\{ l^{\alpha\dagger}_\mu l^\alpha_\mu, \tilde{\rho}_\alpha \right\} \right] \tag{A4}$$

for the effective Markovian dynamics. The number of effective jump operators $\{l^\alpha_\mu\}$ is bounded and does not depend on the system size N (otherwise a mean-field approximation would hardly be legitimate). This is our starting point for the following analysis of nonequilibrium dynamics and steady states.

2. Dynamics

The generic form for single-spin mean-field jump operators is

$$l^\alpha_\mu = \sum_{\lambda=0}^{3} l^\alpha_{\mu,\lambda} \sigma^\lambda_\alpha, \quad \text{where} \quad l^\alpha_{\mu,\lambda} = l^\alpha_{\mu,\lambda}\left(\left\{ m^k_\beta \right\} \right). \tag{A5}$$

Henceforth we use Einstein's convention for Latin indices but not for Greek indices. In the most generic case, jump operators are not traceless, i.e., $l^\alpha_{\mu,0} \neq 0$ (recall that $\sigma^0_\alpha = \mathbb{1}_\alpha$). However, in the models considered here these components vanish altogether and thus we assume $l^\alpha_{\mu,0} = 0$ henceforth. To make this clear, we switch to Latin indices $i,j,k,\ldots$, which run over 1,2,3 (whereas Greek indices run over 0,1,2,3 except for μ, which indicates the different jump operators).

Let us introduce the three-index function

$$L^\alpha_{i,j} \equiv \sum_\mu \overline{l^\alpha_{\mu,i}} l^\alpha_{\mu,j} = R^\alpha_{i,j} + \imath I^\alpha_{i,j} \tag{A6}$$

with real part $R^\alpha_{i,j} = \mathrm{Re} L^\alpha_{i,j}$ and imaginary part $I^\alpha_{i,j} = \mathrm{Im} L^\alpha_{i,j}$. Since $\mathbf{L}^\alpha = (L^\alpha_{i,j})$ is a Hermitian matrix for all α, we find $R^\alpha_{i,j} = R^\alpha_{j,i}$ and $I^\alpha_{i,j} = -I^\alpha_{j,i}$ and thus $R^\alpha \equiv L^\alpha_{i,i} = R^\alpha_{i,i}$. One may call $\mathbf{L}^\alpha$ *system matrices*, as they encode the complete mean-field theory of the system.

Due to the product structure of $\rho^{\mathrm{mf}} = \bigotimes_{\alpha=1}^M \tilde{\rho}_\alpha$ we can parametrize each mean-field density matrix as $\tilde{\rho}_\alpha = 1/2\,(\mathbb{1}_\alpha + a^k_\alpha \sigma^k_\alpha)$. Clearly, self-consistency requires

$$m^k_\alpha = \mathrm{Tr}\left[\sigma^k_\alpha \tilde{\rho}_\alpha\right] = a^k_\alpha \tag{A7}$$

so we can just substitute a^k_α by the expectation value m^k_α, $\tilde{\rho}_\alpha = 1/2\,(\mathbb{1}_\alpha + m^k_\alpha \sigma^k_\alpha)$.

With these definitions in mind it is straightforward to show that the mean-field dynamics, (A4), is described by the set of generally nonlinear differential equations

$$\partial_t m^n_\alpha = 2\epsilon^{ijn} I^\alpha_{i,j} + 2\left(R^\alpha_{n,i} - R^\alpha \delta_{ni}\right) m^i_\alpha, \tag{A8}$$

where δ_{ni} denotes the Kronecker delta and ϵ^{ijn} the Levi-Civita symbol. If we consider all m^n_α ($\alpha = 1,\ldots,M$ and $n = 1,2,3$) as independent real coordinates in $\mathbb{R}^{3M}$, it is convenient to define the vector field

$$\left[F\left(\left\{m^i_\beta\right\}\right)\right]_{(\alpha,n)} \equiv 2\epsilon^{ijn} I^\alpha_{i,j} + 2\left(R^\alpha_{n,i} - R^\alpha \delta_{ni}\right) m^i_\alpha, \tag{A9}$$

which is the flow that determines the time evolution via the dynamical system

$$\partial_t \mathbf{M} = \mathbf{F}, \quad \text{with} \quad \mathbf{M} \equiv \left(m^n_\alpha\right)_{(\alpha,n)}. \tag{A10}$$

For example, in Fig. 2(b) we illustrate the flow $\mathbf{F}$ for the dissipative TIM in the Bloch ball ($M = 1$).

3. Steady states

The mean-field steady states are given by the solutions of $0 \overset{!}{=} \partial_t \mathbf{M} = \mathbf{F}$. Then Eq. (A8) yields the system of generally nonlinear equations

$$R^\alpha m^n_\alpha = \epsilon^{ijn} I^\alpha_{i,j} + m^i_\alpha R^\alpha_{n,i} \tag{A11}$$

for $n = 1,2,3$ and $1 \leqslant \alpha \leqslant M$. Its solutions $(\hat{m}^n_\alpha)$ determine the steady states via $\tilde{\rho}^{\mathrm{NESS}}_\alpha = 1/2\,(\mathbb{1}_\alpha + \hat{m}^k_\alpha \sigma^k_\alpha)$. The stability of these solutions can be inferred from the spectrum $\sigma[\mathrm{D}\mathbf{F}]$ of the derivative (Jacobian matrix $J_{\mathbf{F}}$)

$$\mathrm{D}\mathbf{F} = J_{\mathbf{F}} \equiv \left[\frac{\partial F_{(\alpha,n)}}{\partial m^k_\beta} \right]_{(\alpha,n),(\beta,k)} \tag{A12}$$

at the fixed points $(\hat{m}^n_\alpha)$. A solution with $\max \sigma[\mathrm{D}\mathbf{F}(\hat{m}^n_\alpha)] < 0$ is stable and the corresponding state $\tilde{\rho}^{\mathrm{NESS}}_\alpha$ is considered a physically relevant mean-field steady state. On the contrary, solutions with $\max \sigma[\mathrm{D}\mathbf{F}(\hat{m}^n_\alpha)] > 0$ are not of physical relevance, as their fixed points are unstable at least in one direction of the parameter space $\mathbb{R}^{3M}$.

4. Application to the TIM

Here we consider exemplarily the paradigmatic dissipative TIM. Its competing jump operators are defined in Eq. (3). If we assume a homogeneous system with a single mean-field degree of freedom $m_k \equiv m^k_\alpha = \langle \sigma^k_i \rangle$ for all $1 \leqslant i \leqslant N$, Eq. (A1) yields the ferromagnetic mean-field jump operators (here $p_1 \equiv f_0$; see text)

$$\begin{aligned}
f_1 &= \sigma^x[\mathbb{1} - m_z \sigma^z] \;\Rightarrow\; \mathbf{l}_{f_1} = [1, i m_z, 0], \\
f_2 &= q^{-1/2}\, \overline{m}_z\, \sigma^y \;\Rightarrow\; \mathbf{l}_{f_2} = q^{-1/2}\,[0, \overline{m}_z, 0], \\
f_3 &= q^{-1/2}\, \sigma^z \;\Rightarrow\; \mathbf{l}_{f_3} = q^{-1/2}\,[0,0,1], \\
p_1 &= \sqrt{\kappa}\, \sigma^z[\mathbb{1} - \sigma^x] \;\Rightarrow\; \mathbf{l}_{p_1} = \kappa^{-1/2}/2\,[0, -i, 1],
\end{aligned} \tag{A13}$$

with the coordinate representations $l_{\mu,i}$ ($\mu = f_1, f_2, f_3, p_1$ and $i = 1,2,3$). For the sake of brevity we introduced the coordination number $q \equiv 2D$ and $\overline{m}_z \equiv \sqrt{1-m_z^2}$.

Please note that f_1 and p_1 remain finite in the high-dimensional limit $D \to \infty$, whereas the y- and z-dephasing f_2 and f_3 become irrelevant for high-dimensional systems and affect the results only quantitatively.

We can now evoke Eqs. (A6) and (A9) to derive the mean-field flow in the Bloch ball

$$\mathbf{F}(\mathbf{m}) = \begin{bmatrix} -m_x\left[2\left(\left(1-\frac{1}{q}\right)m_z^2+\frac{2}{q}\right)+\kappa\right]+\kappa \\ -m_y\left[2\left(1+\frac{1}{q}\right)+\frac{\kappa}{2}\right] \\ 2\left(1-\frac{1}{q}\right)m_z\left(1-m_z^2\right)-m_z\frac{\kappa}{2} \end{bmatrix} \tag{A14}$$

with the triangular Jacobian matrix

$$\mathrm{D}\mathbf{F}(\mathbf{m}) = \begin{bmatrix} -2\left[\left(1-\frac{1}{q}\right)m_z^2+\frac{2}{q}\right]-\kappa & 0 & -4m_x m_z\left(1-\frac{1}{q}\right) \\ 0 & -2\left(1+\frac{1}{q}\right)-\frac{\kappa}{2} & 0 \\ 0 & 0 & -2\left(1-\frac{1}{q}\right)\left(3m_z^2-1\right)-\frac{\kappa}{2} \end{bmatrix}, \tag{A15}$$

the spectrum of which can be read off.

Computation of the fixed points $\hat{\mathbf{m}}$ via Eq. (A11)—or, equivalently, $\mathbf{F} = 0$—yields the three solutions

$$\hat{\mathbf{m}}_{\mathrm{P}} = \left[\frac{\kappa q}{\kappa q+4} \quad 0 \quad 0\right]^T, \tag{A16a}$$

$$\hat{\mathbf{m}}_{\mathrm{F1}} = \left[\frac{2\kappa q}{(\kappa+4)q+4} \quad 0 \quad -\frac{1}{2}\sqrt{4-\frac{\kappa q}{q-1}}\right]^T, \tag{A16b}$$

$$\hat{\mathbf{m}}_{\mathrm{F2}} = \left[\frac{2\kappa q}{(\kappa+4)q+4} \quad 0 \quad +\frac{1}{2}\sqrt{4-\frac{\kappa q}{q-1}}\right]^T, \tag{A16c}$$

which can be classified as paramagnetic (P; $\hat{m}_z = 0$) and ferromagnetic (F_1 and F_1; $\hat{m}_z \neq 0$) solutions.

Clearly, the ferromagnetic solutions F_1 and F_2 become real valued (and thereby valid Bloch vectors) iff

$$4-\frac{\kappa q}{q-1} \geqslant 0 \Leftrightarrow \kappa \leqslant \kappa_c \equiv 4\left(1-\frac{1}{q}\right), \tag{A17}$$

where κ_c is the *critical coupling*. We want to stress that $\lim_{D\to\infty}\kappa_c = 4 > 0$; that is, the mean-field phase transition is stable in the high-dimensional limit.

At this point it remains to check which of the three solutions for $\kappa < \kappa_c$ are the physical ones. To this end we have to plug the fixed points in the three eigenvalues of Eq. (A15). This yields, for the paramagnetic solution,

$$\lambda_1^{\mathrm{P}} = 2-\frac{1}{2}\left(\kappa+\frac{4}{q}\right) \lessgtr 0, \quad \lambda_2^{\mathrm{P}} < 0, \quad \lambda_3^{\mathrm{P}} < 0. \tag{A18}$$

We see that $\hat{\mathbf{m}}_{\mathrm{P}}$ becomes unstable for $\kappa < \kappa_c$ since then $\lambda_1^{\mathrm{P}} > 0$. The same procedure for the ferromagnetic solutions yields

$$\lambda_1^{\mathrm{F}} = \kappa-4\left(1-\frac{1}{q}\right) \lessgtr 0, \quad \lambda_2^{\mathrm{F}} < 0, \quad \lambda_3^{\mathrm{F}} < 0, \tag{A19}$$

which leads us to the conclusion that they become stable the moment they become real valued, namely, for $\kappa < \kappa_c$ when λ_1^{F} becomes negative.

These discussions establish the phase diagram in Fig. 2(a) as well as the qualitative structure of the mean-field flow in Fig. 2(b).

APPENDIX B: MEAN-FIELD THEORY FOR THE $\mathbb{Z}_2$-GAUGE-HIGGS MODEL IN UNITARY GAUGE

As brought up above, to properly exclude unphysical (gauge) degrees of freedom, it proves advantageous to localize the latter on distinguished subsystems. These subsystems decouple from the gauge-invariant dynamics and consequently can be dropped in mean-field considerations.

This can be achieved in unitary gauge; here the physical subspace $\mathcal{H}_{\mathbb{Z}_2\mathrm{GH}} = \{|\Psi\rangle \,|\, G_s = \mathbb{1}\}$ is unitarily rotated into the new subspace $\tilde{\mathcal{H}}_{\mathbb{Z}_2\mathrm{GH}} = \{|\Psi\rangle \,|\, \sigma_s^x = \mathbb{1}\} = T\mathcal{H}_{\mathbb{Z}_2\mathrm{GH}}$. The Hermitian and unitary transformation reads

$$T = \prod_{e\in\mathbb{E}}[\mathbb{1}_e P_e^+ + \tilde{I}_e P_e^-], \tag{B1}$$

TABLE II. Jump operators for the dissipative $\mathbb{Z}_2$-Gauge-Higgs model (comparison). Their action is described in the text. Pictorial descriptions are shown in Fig. 3. Subscripts s, e, and p denote sites, edges, and faces, respectively. The shorthand notation $e \in p$ denotes the normalized sum over all edges e adjacent to face p. The free parameters of the theory are labeled η_i for $i = 1,\ldots,6$. The center column lists the jump operators of the gauge theory with nontrivial gauge condition $\sigma_s^x A_s = \mathbb{1}$ (Gauss law). A unitary transformation maps the theory to a new subspace which is defined by the trivial gauge condition $\sigma_s^x = \mathbb{1}$. The jump operators in this subspace (unitary gauge) are listed in the final column. The transformation is described in the text.

	Gauge condition	
Bath	$\sigma_s^x A_s = \mathbb{1}$	$\sigma_s^x = \mathbb{1}$
Gauge string tension	$F_p^{(1)} = \eta_1 B_p(\mathbb{1}-\tau_{e\in p}^x)$	$\tilde{F}_p^{(1)} = \eta_1 B_p(\mathbb{1}-\tau_{e\in p}^x)$
Gauge string fragility	$F_e^{(2)} = \eta_2 I_e(\mathbb{1}-\tau_e^x)$	$\tilde{F}_e^{(2)} = \eta_2\tau_e^z(\mathbb{1}-\tau_e^x)$
Higgs brane tension	$D_s^{(1)} = \eta_3\sigma_s^x(\mathbb{1}-I_{e\in s})$	$\tilde{D}_s^{(1)} = \eta_3 A_s(\mathbb{1}-\tau_{e\in s}^z)$
Higgs brane fragility	$D_e^{(2)} = \eta_4\tau_e^x(\mathbb{1}-I_e)$	$\tilde{D}_e^{(2)} = \eta_4\tau_e^x(\mathbb{1}-\tau_e^z)$
Charge hopping & annihilation	$T_e = \eta_5 I_e(\mathbb{1}-\sigma_{s\in e}^x)$	$\tilde{T}_e = \eta_5\tau_e^z(\mathbb{1}-A_{s\in e})$
Flux string tension	$B_e = \eta_6\tau_e^x(\mathbb{1}-B_{p\in e})$	$\tilde{B}_e = \eta_6\tau_e^x(\mathbb{1}-B_{p\in e})$

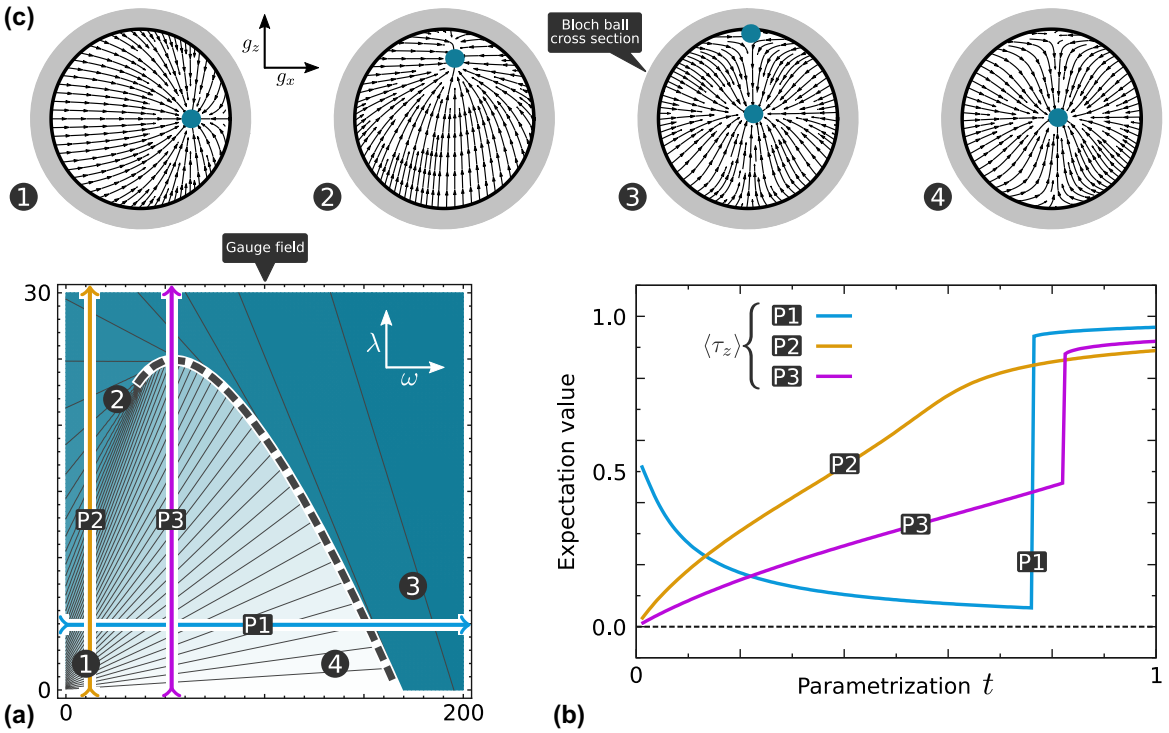

FIG. 6. (Color online) Mean-field phase diagram for the dissipative $\mathbb{Z}_2$-Gauge-Higgs model in unitary gauge. (a) Plot of the maximal z polarization $\langle \tau^z \rangle$ of all stable physical steady states color-coded in the ω-λ plane (light $\rightarrow \langle \tau^z \rangle = 0$, dark $\rightarrow \langle \tau^z \rangle = 1$). (b) Quantitative results for $\langle \tau^z \rangle$ on the colored and labeled paths in (a). (c) Four characteristic cross sections of the Bloch ball (g_x-g_z plane) with the dynamical mean-field flow **F** as flux lines and the stable physical fixed points shown by cyan circles. The corresponding parameters (ω,λ) for each cross section are highlighted by numbers in the 2D plot (a). A discussion of the results is given in the text.

with the projectors $P_e^{\pm} = \frac{1}{2}(\mathbb{1}_e \pm \tau_e^x)$ and the operator $\tilde{I}_{e=(st)} \equiv \sigma_s^z \sigma_t^z$. To transform the jump operators, it is useful first to show that

$$T\tau_e^z T^\dagger = I_e, \quad T\tau_e^x T^\dagger = \tau_e^x,$$
$$T\sigma_s^z T^\dagger = \sigma_s^z, \quad T\sigma_s^x T^\dagger = G_s$$

and then to calculate $\tilde{L} = TLT^\dagger$; this yields the unitary gauge representation in the final column in Table II. The gauge condition becomes trivial, $\sigma_s^x = \mathbb{1}$, and can be accounted for by just dropping the matter field completely, as it does not enter the dynamics. This establishes a one-to-one correspondence between mathematical and physical degrees of freedom which prevents the mean-field theory from taking into account the unphysical ones. To this end, we make the ansatz $\rho = \bigotimes_{e\in\mathbb{E}} \rho_e^g$ and derive once again the (now three-dimensional) dynamical mean-field flow $\mathbf{F}(\mathbf{g})$.

The results are illustrated in Fig. 6. In accordance with the mean-field theory for the Hamiltonian counterpart, the distinction between the Higgs and the free charge phase is lost, whereas the analytical path between the confined charge and the Higgs phase is recovered [Fig. 6(a)]. The phase transition separating the confined charge and free charge and Higgs phases is still discontinuous as Fig. 6(b) reveals. In contrast to the mean-field approach discussed above, the flow $\mathbf{F}(\mathbf{g})$ is only three-dimensional and we can illustrate its topology faithfully in the Bloch ball cross sections [Fig. 6(c)]. Note that the $g_z > 0$ solution is indeed stable since there is a nearby unstable fixed point separating the stable $g_z > 0$ and $g_z = 0$ solutions. The cross sections illustrate nicely how the topology of the mean-field flow gives rise to the continuous transition connecting the two phases: When the discontinuous phase boundary is traversed from (4) to (3), the $g_z = 0$ solution remains at the center of the Bloch ball, while close to the $g_z = 1$ pole two new fixed points (one stable, one unstable) emerge. When, in contrast, the continuous path along (2) is taken, the single stable solution approaches the pole until it "splits" into a pair of stable fixed points and an unstable fixed point; one stable fixed point approaches the pole, while the other seeks the center of the Bloch ball.

[1] F. Verstraete, M. M. Wolf, and J. I. Cirac, Quantum computation and quantum-state engineering driven by dissipation, Nature Phys. **5**, 633 (2009).

[2] F. Pastawski, L. Clemente, and J. I. Cirac, Quantum memories based on engineered dissipation, Phys. Rev. A **83**, 012304 (2011).

[3] B. Kraus, H. P. Buchler, S. Diehl, A. Kantian, A. Micheli, and P. Zoller, Preparation of entangled states by quantum Markov processes, Phys. Rev. A **78**, 042307 (2008).

[4] H. Weimer, M. Müller, I. Lesanovsky, P. Zoller, and H. P. Büchler, A Rydberg quantum simulator, Nature Phys. **6**, 382 (2010).

[5] F. Ticozzi and L. Viola, Steady-state entanglement by engineered quasi-local Markovian dissipation: Hamiltonian-assisted and conditional stabilization, Quantum Info. Comput. **14**, 265 (2014).

[6] J. T. Barreiro *et al.*, An open-system quantum simulator with trapped ions, Nature **470**, 486 (2011).

[7] P. Schindler *et al.*, Quantum simulation of dynamical maps with trapped ions, Nature Phys. **9**, 361 (2013).

[8] S. Diehl *et al.*, Quantum states and phases in driven open quantum systems with cold atoms, Nature Phys. **4**, 878 (2008).

[9] T. Prosen and I. Pižorn, Quantum phase transition in a far-from-equilibrium steady state of an XY spin chain, Phys. Rev. Lett. **101**, 105701 (2008).

[10] S. Diehl, A. Tomadin, A. Micheli, R. Fazio, and P. Zoller, Dynamical phase transitions and instabilities in open atomic many-body systems, Phys. Rev. Lett. **105**, 015702 (2010).

[11] J. Eisert and T. Prosen, Noise-driven quantum criticality, arXiv:1012.5013v1.

[12] A. Tomadin, S. Diehl, and P. Zoller, Nonequilibrium phase diagram of a driven and dissipative many-body system, Phys. Rev. A **83**, 013611 (2011).

[13] T. E. Lee, H. Häffner, and M. C. Cross, Antiferromagnetic phase transition in a nonequilibrium lattice of Rydberg atoms, Phys. Rev. A **84**, 031402 (2011).

[14] M. Foss-Feig, K. R. A. Hazzard, J. J. Bollinger, and A. M. Rey, Nonequilibrium dynamics of arbitrary-range Ising models with decoherence: An exact analytic solution. Phys. Rev. A **87**, 042101 (2013).

[15] M. Höning, M. Moos, and M. Fleischhauer, Critical exponents of steady-state phase transitions in fermionic lattice models, Phys. Rev. A **86**, 013606 (2012).

[16] C. Ates, B. Olmos, J. P. Garrahan, and I. Lesanovsky, Dynamical phases and intermittency of the dissipative quantum Ising model, Phys. Rev. A **85**, 043620 (2012).

[17] E. M. Kessler, G. Giedke, A. Imamoglu, S. F. Yelin, M. D. Lukin, and J. I. Cirac, Dissipative phase transition in a central spin system, Phys. Rev. A **86**, 012116 (2012).

[18] T. Shirai, T. Mori, and S. Miyashita, Novel symmetry-broken phase in a driven cavity system in the thermodynamic limit, J. Phys. B: At. Mol. Phys. **47**, 025501 (2014).

[19] I. Lesanovsky, M. van Horssen, M. Gutua, and J. P. Garrahan, Characterization of dynamical phase transitions in quantum jump trajectories beyond the properties of the stationary state, Phys. Rev. Lett. **110**, 150401 (2013).

[20] L. Banchi, P. Giorda, and P. Zanardi, Quantum information-geometry of dissipative quantum phase transitions, Phys. Rev. E **89**, 022102 (2014).

[21] M. Hoening, W. Abdussalam, M. Fleischhauer, and T. Pohl, Antiferromagnetic long-range order in dissipative Rydberg lattices, Phys. Rev. A **90**, 021603 (2014).

[22] G. Lindblad, On the generators of quantum dynamical semigroups, Commun. Math. Phys. **48**, 119 (1976).

[23] M. B. Plenio and P. L. Knight, The quantum-jump approach to dissipative dynamics in quantum optics. Rev. Modern Phys. **70**, 101 (1998).

[24] R. P. Feynman, Simulating physics with computers, Int. J. Theor. Phys. **21**, 467 (1982).

[25] S. Lloyd, Universal quantum simulators, Science **273**, 1073 (1996).

[26] S. Sachdev, *Quantum Phase Transitions* (Cambridge University Press, Cambridge, UK, 2011).

[27] This is easy to see since there is no common pure state in the kernels of all jump operators P_s and F_s.

[28] J. Dalibard, Y. Castin, and K. Mølmer, Wave-function approach to dissipative processes in quantum optics, Phys. Rev. Lett. **68**, 580 (1992).

[29] R. Dum, P. Zoller, and H. Ritsch, Monte Carlo simulation of the atomic master equation for spontaneous emission, Phys. Rev. A **45**, 4879 (1992).

[30] T. E. Lee, H. Häffner, and M. C. Cross, Collective quantum jumps of Rydberg atoms, Phys. Rev. Lett. **108**, 023602 (2012).

[31] F. J. Wegner, Duality in generalized Ising models and phase transitions without local order parameters, J. Math. Phys. **12**, 2259 (1971).

[32] E. Fradkin and L. Susskind, Order and disorder in gauge systems and magnets, Phys. Rev. D **17**, 2637 (1978).

[33] E. Fradkin and S. H. Shenker, Phase diagrams of lattice gauge theories with Higgs fields, Phys. Rev. D **19**, 3682 (1979).

[34] E. Zohar, J. I. Cirac, and B. Reznik, Quantum simulations of gauge theories with ultracold atoms: Local gauge invariance from angular-momentum conservation, Phys. Rev. A **88**, 023617 (2013).

[35] K. Stannigel, P. Hauke, D. Marcos, M. Hafezi, S. Diehl, M. Dalmonte, and P. Zoller, Constrained dynamics via the zeno effect in quantum simulation: Implementing non-Abelian lattice gauge theories with cold atoms, Phys. Rev. Lett. **112**, 120406 (2014).

[36] D. Marcos *et al.*, Two-dimensional lattice gauge theories with superconducting quantum circuits, Ann. Phys. **351**, 634 (2014).

[37] I. S. Tupitsyn, A. Kitaev, N. V. Prokofev, and P. C. E. Stamp, Topological multicritical point in the phase diagram of the toric code model and three-dimensional lattice gauge Higgs model, Phys. Rev. B **82**, 085114 (2010).

[38] The deconfinement of *both*, charges and fluxes, in two spatial dimensions is directly related to the thermal instability of the toric code.

[39] J.-M. Drouffe and J.-B. Zuber, Strong coupling and mean field methods in lattice gauge theories, Phys. Rep. **102**, 1 (1983).

[40] E. Dagotto, An improved mean-field calculation for the $Z(2)$ Higgs model, Phys. Lett. B **136**, 60 (1984).

[41] J. M. Alvarez and H. M. Socolovsky, Mean-field approximation for Z_N lattice gauge theory coupled to matter, Nuovo Cimento A **90**, 31 (1985).

[42] For instance, consider the $\mathbb{Z}_2$-Gauge-Higgs model. Here one naturally introduces two mean fields for the gauge and the matter field, respectively.